Earth and Planetary Science Letters 443 (2016) 59–69

Contents lists available at ScienceDirect

Earth and Planetary Science Letters

www.elsevier.com/locate/epsl

Temperature dependence of basalt weathering

Gaojun Li [a,*], Jens Hartmann [b], Louis A. Derry [c], A. Joshua West [d], Chen-Feng You [e], Xiaoyong Long [f], Tao Zhan [g], Laifeng Li [a], Gen Li [d], Wenhong Qiu [a], Tao Li [a], Lianwen Liu [a], Yang Chen [a], Junfeng Ji [a], Liang Zhao [a], Jun Chen [a]

[a] MOE Key Laboratory of Surficial Geochemistry, Department of Earth Sciences, Nanjing University, 163 Xianlindadao, Nanjing 210023, China
[b] Institute for Geology, Center for Earth System Research and Sustainability (CEN), Universität Hamburg, Bundesstrasse 55, D-20146 Hamburg, Germany
[c] Department of Earth and Atmospheric Sciences, Cornell University, Ithaca, NY 14853, USA
[d] Department of Earth Sciences, University of Southern California, 3651 Trousdale Parkway, Los Angeles, CA 90089, USA
[e] Earth Dynamic System Research Center, National Cheng Kung University, Tainan 70101, Taiwan
[f] College of Geographical Science, Southwest University, 1 Tiansheng Road, Chongqing 400715, China
[g] The Second Hydrogeology and Engineering Geology Prospecting Institute of Heilongjiang Province, Harbin 150030, China

ARTICLE INFO

Article history:
Received 24 April 2015
Received in revised form 4 March 2016
Accepted 8 March 2016
Available online 24 March 2016
Editor: M. Bickle

Keywords:
chemical weathering
erosion
climate change
volcano
river chemistry

ABSTRACT

The homeostatic balance of Earth's long-term carbon cycle and the equable state of Earth's climate are maintained by negative feedbacks between the levels of atmospheric CO_2 and the chemical weathering rate of silicate rocks. Though clearly demonstrated by well-controlled laboratory dissolution experiments, the temperature dependence of silicate weathering rates, hypothesized to play a central role in these weathering feedbacks, has been difficult to quantify clearly in natural settings at landscape scale. By compiling data from basaltic catchments worldwide and considering only inactive volcanic fields (IVFs), here we show that the rate of CO_2 consumption associated with the weathering of basaltic rocks is strongly correlated with mean annual temperature (MAT) as predicted by chemical kinetics. Relations between temperature and CO_2 consumption rate for active volcanic fields (AVFs) are complicated by other factors such as eruption age, hydrothermal activity, and hydrological complexities. On the basis of this updated data compilation we are not able to distinguish whether or not there is a significant runoff control on basalt weathering rates. Nonetheless, the simple temperature control as observed in this global dataset implies that basalt weathering could be an effective mechanism for Earth to modulate long-term carbon cycle perturbations.

1. Introduction

The control of climate on the rate of silicate mineral weathering and thus the burial of atmospheric CO_2 in carbonate minerals over geologic time provides a negative feedback stabilizing changes in Earth's atmospheric CO_2 concentration (pCO_2). Such a pCO_2-weathering feedback is believed to have maintained the homeostatic balance of the long-term carbon cycle and the habitability of Earth's surface over timescales $>\sim 10^5$ yrs (Walker et al., 1981; Berner et al., 1983; MacKenzie and Andersson, 2013). The limited reservoir of carbon in the atmosphere and oceans implies that disturbances in carbon cycle fluxes will result in changes in pCO_2, and thus climate through the greenhouse effect of CO_2. Changing climate will drive changes in the consumption of CO_2 by weathering, opposite to the direction of initial change, until carbon fluxes into and out of the atmosphere–ocean system are balanced and a new equilibrium is established (Berner and Caldeira, 1997).

The temperature dependence of silicate mineral weathering rates is believed to have played an important role in the pCO_2-weathering feedbacks together with the effects of runoff and biotic interactions (e.g., Berner and Kothavala, 2001; Arvidson et al., 2006). As predicted by chemical kinetics, rates of mineral dissolution show distinct temperature dependence in well-controlled lab experiments (Kump et al., 2000). Although there is also evidence for the temperature dependence of silicate weathering fluxes in field settings (White and Blum, 1995; Oliva et al., 2003), the inferred relationships are often complicated by multiple effects on weathering. Some of the other factors that might influence field-scale weathering fluxes, such as precipitation, runoff, and vegetation, co-vary with temperature, and the importance of variations in erosion rate further confounds simple interpretation (Riebe et al., 2004; West et al., 2005; Ferrier and Kirchner, 2008; Dixon et al., 2012; West, 2012). Moreover, natural weathering sys-

* Corresponding author.
E-mail address: ligaojun@nju.edu.cn (G. Li).

http://dx.doi.org/10.1016/j.epsl.2016.03.015

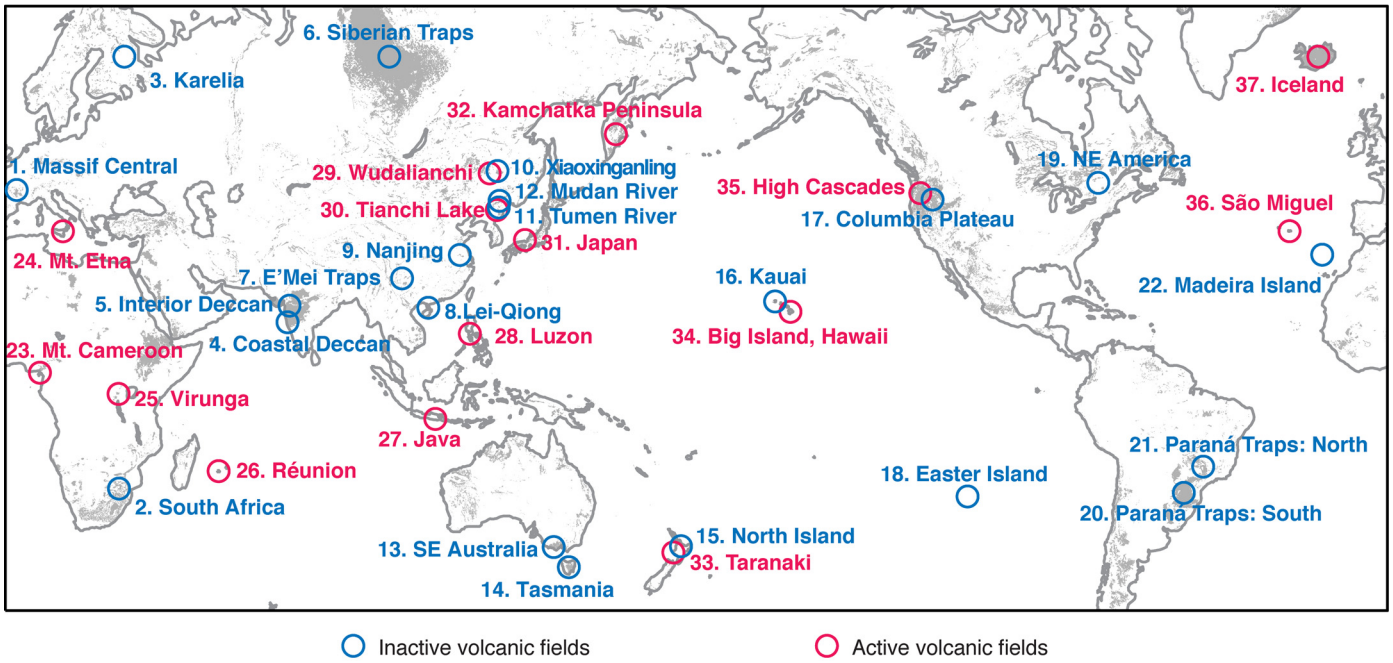

Fig. 1. Distribution of the basaltic fields in our compilation. Shaded area shows the distribution of basaltic rocks based on global lithological map (Hartmann and Moosdorf, 2012). Red and blue circles are for active and inactive basaltic fields, respectively. (For interpretation of the references to color in this figure legend, the reader is referred to the web version of this article.)

tems that approach equilibrium will be controlled by thermodynamic rather than kinetic limits, with greater importance of water flow than temperature in controlling total alkalinity fluxes that consume CO_2 (Maher, 2011).

Studies on single lithologies may reduce the complexities associated with rock types (White and Blum, 1995; Oliva et al., 2003; Hartmann, 2009; Ferrier et al., 2012). The relatively homogeneous composition among geographic regions makes basaltic rocks an ideal target for such investigation (Bluth and Kump, 1994). Previous studies have demonstrated that basalt weathering is globally significant due to rapid weathering rates and the resulting large global weathering fluxes, despite limited areal coverage of basalts (Gislason et al., 1996; Louvat and Allègre, 1997, 1998; Gaillardet et al., 1999; Dessert et al., 2003; Schopka et al., 2011. An empirically observed relationship between mean annual temperature (MAT, in °C) and the concentration of dissolved bicarbonate (resembling alkalinity) in stream water draining basaltic rocks has been proposed (Dessert et al., 2003):

$$K_{CO_2} = RUN \times C = RUN \times c_2 e^{c_1 MAT} \quad (1)$$

where K_{CO_2} (mol/km^2/yr) is the consumption rate of atmospheric CO_2 associated with basalt weathering, *RUN* (mm/yr) the annual runoff, C (μmol/L) the concentration of bicarbonate in stream water, and c_1 (1/°C) and c_2 (μmol/L) the constants that define the empirical relationship between temperature and concentration of bicarbonate. Such mathematical laws are the basic building blocks of numerical models calculating the evolution of the partial pressure of atmospheric CO_2 and Earth's climate over geological timescales (e.g., Berner et al., 1983; Donnadieu et al., 2006; Goddéris et al., 2014; Mills et al., 2014).

The model of Dessert et al. (2003) provides a first-order description of basalt weathering but does not account for some important observations. One such observation is that dilution with increasing runoff has been widely recognized for basaltic rivers (Bluth and Kump, 1994). In contrast, the model of Dessert et al. (2003) requires that the concentrations of bicarbonate are independent of runoff (Eq. (1)).

Another observation not explicitly considered in the model of Dessert et al. (2003) is that emplacement age of basaltic rocks influences observed weathering fluxes, with younger volcanic fields showing higher weathering reactivity (Bluth and Kump, 1994; Amiotte-Suchet and Probst, 1995; Louvat et al., 2008; Hartmann, 2009; Rad et al., 2013; Freire et al., 2014). Several potential mechanisms, operating at different scales, could explain why weathering rates are influenced by emplacement age. At the scale of mineral surfaces, changes in surface area, etch pit size and density, and coatings of secondary phases can impact mineral dissolution rates (White and Brantley, 2003). At the catchment scale, regolith development can change hydraulic conductivity with consequent changes in infiltration rates and surface water–ground water partitioning (Lohse and Dietrich, 2005; Schopka and Derry, 2012). At the scale of the volcanic edifice, active volcanic fields commonly support hydrothermal circulation as well as degassing of CO_2, SO_2, and other reactive gases. Volcanic CO_2 degassing can contribute significantly to the alkalinity fluxes from active volcanic centers (Aiuppa et al., 2000; Rivé et al., 2013).

New observations on the chemistry of rivers draining basaltic fields provide an opportunity to update prior compilations (Dessert et al., 2003) and re-examine the relationships between basalt weathering and climatic factors. In this study, we compile data from 37 basaltic regions based on published datasets, together with new data from several Chinese basaltic fields (Fig. 1). We separate the data compilation into 22 inactive volcanic fields (IVFs) and 15 active volcanic fields (AVFs) and find that the role of temperature is clarified if only IVFs are considered (Fig. 2(a)).

2. Methods

2.1. Proxy for weathering rate

Estimation of weathering rates relies on using the mineral–water interfacial area as a scaling factor (Navarre-Sitchler and Brantley, 2007). Rates inferred from the flux of weathering-derived dissolved ions in a river are typically normalized to the geographic surface area of the river catchment. Following Dessert et al. (2001),

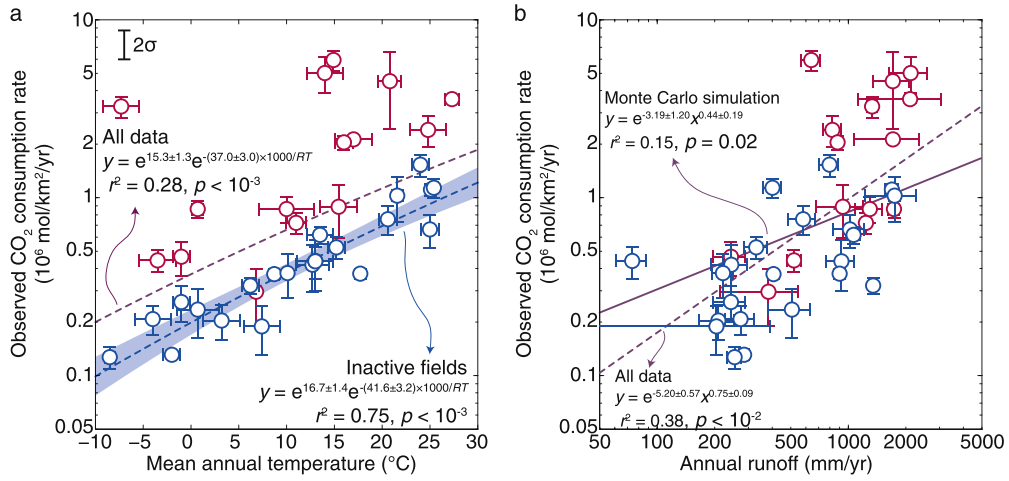

Fig. 2. Cross-plots between CO_2 consumption rate and climate factors. (a) Cross-plot between CO_2 consumption rate and temperature. The regression lines are for all data and inactive volcanic fields. Shaded area is 95% confidence band of the Monte Carlo simulation for inactive volcanic fields. No significant correlation is found for active volcanic fields alone ($p > 0.05$). (b) Cross-plot between runoff and CO_2 consumption rate. Significant correlation is found for all data considered together, but not for the data from active and inactive volcanic fields separately. Also shown in (b) is the result of Monte Carlo simulation that explains the correlation by the uncertainties of runoff and the high runoff of active volcanic fields. Error bars show 2× standard deviation of the mean ($2\sigma_m$). Labels are the same as those in Fig. 1.

the flux of bicarbonate is used as an index for basalt weathering because the dissolved bicarbonate in river water is mainly derived from weathering reactions and the influence of rainwater and anthropogenic input on riverine bicarbonate flux is less important compared to other chemical constituents. In this case, the rate of CO_2 consumption by basalt weathering (K_{CO_2}) can be calculated by multiplying the mean concentration of dissolved inorganic carbon (DIC, C) by annual runoff (*RUN*) as expressed in Eq. (1). For simplicity, we assume that the concentration of DIC is the same as that of alkalinity or bicarbonate because bicarbonate is the largest contributor to alkalinity and DIC in the typical *p*H range of natural river water.

In arid to semi-arid settings, pedogenic carbonate can form as a result of basalt weathering, and later dissolution of this carbonate contributes to measured DIC flux. Some studies have reported K_{CO_2} based on the concentration of cations derived from silicate weathering rather than the simple DIC flux to correct the contribution from the weathering of pedogenic carbonate minerals (Sharma and Subramanian, 2008; Gupta et al., 2011). In basaltic weathering profiles much of the Ca^{2+} in pedogenic carbonate is basalt-derived, even in settings with significant marine aerosol inputs (Capo et al., 2000; Trostle et al., 2014). Similarly, carbonates precipitated from hydrothermal fluids in silicate terranes contain cations derived from silicate alteration (Evans et al., 2004; Jacobson et al., 2015). Later weathering of either pedogenic or hydrothermal carbonate contributes alkalinity that is originally derived from alteration of silicates, despite temporary residence in a carbonate phase (Evans et al., 2001). The transient formation and later dissolution of carbonate, which is likely to take place on timescales of $\sim 10^2$–10^5 yrs (Kelemen and Matter, 2008; Matter and Kelemen, 2009; Mervine et al., 2014), is unlike longer-term ($>\sim 10^6$ yr timescale) recycling of sedimentary carbonate that results in no net long-term CO_2 consumption. Because the transient carbonate is derived from silicate sources within the last $\sim 10^2$–10^5 yrs, release of the associated cations to rivers and the oceans will affect long-term CO_2. Though this study includes only data from catchments that do not have sedimentary carbonates, pedogenic and hydrothermal carbonates are present in at least some of the catchments. We do not attempt to adjust for the contribution from these "basaltic carbonates". In some cases input from atmospheric deposition to this carbonate reservoir may result in a slight overestimate of the silicate weathering flux by using bicarbonate data, but eliminating all carbonate-derived alkalinity would result in a larger underestimate of the relevant CO_2 flux, since most of the hydrothermal and pedogenic carbonate from basaltic settings is ultimately of silicate origin.

The calculation of silicate weathering-derived cation budgets may also introduce additional uncertainties due to the contribution of rainfall (sea salt), sulphuric acid weathering, and anthropogenic pollution to the cations. These inputs are not readily corrected in many cases (Gaillardet et al., 1999). We do not use dissolved Si as index for basalt weathering because dissolved Si can be significantly influenced by the precipitation and dissolution of biogenic opal (Conley, 2002; Derry et al., 2005; Harrison et al., 2012) and other secondary phases.

We also do not separate the high temperature hydrothermal weathering component from the total weathering flux. Irrespective of the source of CO_2, fluid–rock interaction at hydrothermal temperatures ("high *T* weathering"; Evans et al., 2001) will be faster and often more complete (e.g. closer to achieving equilibrium) than that at ambient surface temperatures. The geological-scale CO_2 consumption from silicate alteration does not depend on the source of CO_2, e.g. whether the CO_2 involved in the weathering reaction is derived from the atmosphere, soil respiration, or directly from volcanic sources. Nor does it depend on the locus or temperature of reaction as long as CO_2 that otherwise would be made available to the ocean–atmosphere system is instead converted to alkalinity that can be transported to the oceans and removed as carbonate minerals (Evans et al., 2004; Rivé et al., 2013). At the timescale of interest for long-term regulation of the climate system we can consider these processes as equivalent, and it is not necessary to deconvolve the sources of CO_2 that generate the silicate-derived alkalinity flux. However, we do note that the hydrothermal activity associated with AVFs may complicate interpretation of the temperature dependence of inferred weathering rates (see discussion in Section 4.3).

2.2. Strategies of data compilation

Detailed site-by-site description of the data compilation is provided in the supplementary material. An overview of the approach used in assembling this compilation is provided here. The data either came from published literature or from the GLObal RIver CHemistry database (GLORICH) database (Hartmann et al., 2014a). Many of the data from literature sources were previously compiled by Dessert et al. (2003); data from the same sites are fur-

ther updated here with more recently available information. The GLORICH database combines an assemblage of hydrochemical data from varying sources (Hartmann et al., 2014a), together with the properties of each catchment, including catchment size, lithology, and climate. The database comprises 1.27 million samples distributed over 17 000 sampling locations. The mean annual temperature (MAT) of the catchments in this database is derived from WorldClim (Hijmans et al., 2005). Annual runoff is derived from the UNH/GRDC runoff composites (Fekete et al., 2002), which has 30-minute spatial resolution. Model bias in the UNH/GRDC runoff composites is basin area-dependent, and the model tends to overestimate runoff in basins on the order of 10^4 km^2 or smaller (Fekete et al., 2002). Most of the basaltic catchments in the GLORICH database are smaller than 10^4 km^2, so runoff values may be overestimated for these locations.

Only catchments with dominantly basaltic lithology have been selected in this compilation. Thus, andesitic fields such as those extensively researched in Lesser Antilles are not included (Goldsmith et al., 2010; Gaillardet et al., 2011; Lloret et al., 2011; Rad et al., 2013; Rivé et al., 2013). We also exclude catchments where basaltic lithology is mapped as covering <80% of the catchment surface area because calculation of basaltic weathering flux in mixed lithology may introduce large uncertainty (Gaillardet et al., 2003). One exception is made for the Karelia region, where weathering fluxes and concentrations of DIC correlate well with the fraction of area covered by basaltic rock, and the highest basaltic coverage is >80% (Zakharova et al., 2007). Thus, extrapolation can be accurately made to infer the weathering flux of pure basaltic catchments from this region.

Chemical fluxes carried by ground water are considered where data are available because recent work shows considerable direct groundwater discharge to the oceans from volcanic islands (e.g., Schopka and Derry, 2012). We think the contribution of ground water discharge is important for active volcanic fields because the drainage system has not been well developed in these young geomorphological settings (Jefferson et al., 2010). For aged basaltic fields where rivers cut deeply into the bedrock, a large portion of ground water discharge has already been accounted for in the surface flow of lower river reaches.

MAT is used to represent the regional differences in temperature. We take MAT as an appropriate proxy for the average temperature of weathering reactions because soil temperature roughly follows MAT (Ferrier et al., 2012). However, the weathering flux may be biased to warm seasons due to the exponential dependence of weathering rate on the temperature (Lasaga et al., 1994). In addition, it should be noticed that several catchments in high latitudes have MAT lower than 0 °C, a temperature below which no liquid water is available for weathering reaction. Thus, MAT should be regarded as a proxy for the relative difference of temperature between catchments rather than the absolute temperature of weathering reactions (Lasaga et al., 1994).

The largest uncertainties in our compilation are associated with runoff and concentration of DIC due to the temporal and spatial resolution of the data. Runoff based on temporally resolved measurement of river flow is the most reliable. However, such data is unavailable for many small catchments. In these cases, runoff data is derived from long-term observation of nearby rivers, from global runoff models (Fekete et al., 2002), or from local hydrological reports. Concentration of DIC in small catchments generally shows large spatial and temporal variations. We think the use of data from large rivers and averaging of the temporal and spatial data may reduce such uncertainties. To maximize the representativeness, only mainstream data from the downstream location in each catchment is used (when such data is available) instead of headwater data. Two basaltic regions from the GLORICH database are ignored (ID: 300710 in Östvallen, Sweden and ID: 301736 in the Freisbach, Germany) because only one data point from a single small catchment is available, so values for these sites may have large uncertainty.

The data compilation has several layers of averaging. Weighted averages using water flux as weighting factors are used for the concentration of DIC, and weighted averages using catchment area as weighting factors are used for MAT and K_{CO_2} if discharge and catchment area are available. Otherwise, arithmetic averaging is used. Details on the data compilation (along with the new data from several Chinese basaltic fields) can be found in the supplementary material. The final results are listed in Table 1. The data is organized according to geographic location since the catchments in the same basaltic fields generally have similar climatic condition and emplacement age. For large basaltic fields, such as the Deccan Traps and the Paraná Traps, which have heterogeneous climate, data are also organized by climatic region. The basaltic catchments are separated into two groups, AVFs and IVFs, according to the presence of identified volcanic or hydrothermal activity. Aged volcanoes (which we classify as IVFs) are defined as those that are dormant and do not have hydrothermal activity.

2.3. Uncertainties

The estimation of uncertainties was conducted case by case due to the varying types of data source. Standard deviations of the mean (σ_m) were used to quantify the uncertainties listed in Table 1. In most cases, σ_m was calculated during the process of averaging the data. In the other cases, a generic error was estimated. Details on σ_m estimation for each case can be found in the supplementary material.

Estimates of MAT, based on either climate maps or local weather stations, are relatively accurate because inter-annual variability of MAT is small relative to the range of values across catchments. Some uncertainty in MAT may arise from spatial variability within catchments. The MAT of each catchment in the GLORICH data base has already been integrated across each catchment area using the WorldClim temperature map (Hijmans et al., 2005) and catchment areas delineated in GIS based on a global digital elevation model, or DEM (Hartmann et al., 2014a). For catchments with MAT estimated from local weather stations, there may be larger uncertainty because of the elevation offset between the weather station and the catchment, and variation of elevation within the catchment. In these cases, the average MAT of the catchment can be roughly calibrated using the offset between mean catchment elevation and the elevation of the nearest weather stations assuming a standard temperature lapse rate of ~6.5 °C/km. The catchments with the largest uncertainty in MAT are those with the largest elevation ranges. Nevertheless, the average σ_m of MAT is 1.2 °C (ranging from 0.1 to 3 °C), which is relatively small compared to the overall variation between catchments of 36 °C.

The mean coefficient of variation (CV, σ_m/mean × 100%) of DIC concentration is 19% even through the temporal resolution of the samples for many regions is low. This is probably because of the quasi-chemostatic behavior of river water in general (Bluth and Kump, 1994). The mean σ_m of runoff is 19%. Interestingly, the mean CV of K_{CO_2}, which should accumulate the uncertainties of bicarbonate concentration and runoff, is only 20%. This is probably because concentrations of DIC are negatively correlated with runoff in many regions, so variation in calculated K_{CO_2} is reduced.

2.4. Statistics

Correlations between observed K_{CO_2}, DIC concentration (C), and climate factors (*MAT* and *RUN*) were evaluated based on physically based functional relationships and the empirical basalt weathering law of Dessert et al. (2003), i.e., Eq. (1) (see Table 2 for summary

Table 1
Summary of data compilation.

Site[a]	MAT (°C)		Runoff (mm/yr)		HCO_3^- (μmol/L)		K_{CO_2} (10^6 mol/km^2/yr)	
	Mean	σ_m	Mean	σ_m	Mean	σ_m	Mean	σ_m
Inactive volcanic fields								
1. Massif Central	8.70	0.65	406	20	916	46	0.372	0.026
2. South Africa	12.70	1.80	244	55	1728	1078	0.420	0.130
3. Karelia	−2.00	1.00	285	20	460	41	0.131	0.007
4. Coastal Deccan	25.10	0.50	1690	150	657	17	1.110	0.103
5. Interior Deccan	25.40	0.50	401	48	2839	170	1.138	0.152
6. Siberian Traps	−8.50	0.65	254	25	501	89	0.127	0.019
7. E'Mei	6.20	1.00	1350	75	238	23	0.321	0.036
8. Lei-Qiong	24.00	1.00	797	100	1923	165	1.532	0.233
9. Nanjing	15.20	1.00	330	48	1595	63	0.526	0.079
10. Xiaoxinganling	−1.00	1.00	243	50	1065	132	0.259	0.062
11. Tumen River	−4.00	2.00	273	50	763	50	0.208	0.041
12. Mudan River	3.20	2.00	209	46	977	87	0.204	0.048
13. SE Australia	13.00	0.10	74	14	5956	657	0.441	0.097
14. Tasmania	10.10	0.25	221	30	1704	437	0.377	0.109
15. North Island	13.00	2.00	920	161	478	131	0.439	0.143
16. Kauai, Hawaii	21.58	0.65	1747	539	588	251	1.026	0.303
17. Columbia Plateau	7.40	2.00	204	191	927	215	0.189	0.060
18. Easter Island	20.60	1.00	580	100	1306	132	0.757	0.151
19. NE America	0.70	2.30	507	129	465	316	0.235	0.075
20. Paraná Traps: South	17.70	0.27	900	27	416	26	0.374	0.027
21. Paraná Traps: North	25.00	1.00	1020	200	651	72	0.664	0.149
22. Madeira Island	13.50	1.50	1065	100	580	43	0.618	0.074
Active volcanic fields								
23. Mt. Cameroon	14.00	2.00	2120	500	2368	110	5.020	1.207
24. Mt. Etna	14.90	0.20	640	80	9286	539	5.943	0.819
25. Virunga	20.80	1.30	1709	380	2646	1757	4.522	2.110
26. Réunion	17.00	2.00	1712	652	1243	290	2.127	0.031
27. Java	24.80	2.00	826	100	2913	500	2.405	0.505
28. Luzon	27.30	0.80	2106	990	1700	806	3.580	0.230
29. Wudalianchi Lake	−1.00	1.00	243	50	1919	190	0.466	0.106
30. Tianchi Lake	−7.30	2.00	1332	100	2445	300	3.258	0.469
31. Japan	10.99	1.12	1236	64	584	73	0.722	0.107
32. Kamchatka Peninsula	−3.50	2.00	520	50	854	100	0.444	0.067
33. Taranaki	10.00	3.00	1296	223	667	34	0.864	0.155
34. Big Island, Hawaii	15.44	2.00	935	269	951	424	0.889	0.303
35. High Cascades	6.81	0.47	382	172	776	175	0.296	0.108
36. São Miguel	16.00	1.00	879	50	2331	200	2.047	0.211
37. Iceland	0.70	0.65	1734	136	498	74	0.864	0.109

[a] Data source: 1 (Meybeck, 1986; Négrel and Deschamps, 1996); 2, 13, 14, 19, 20, 31, 35 (Hartmann et al., 2014a); 3 (Zakharova et al., 2007); 4 (Das et al., 2005); 5 (Dessert et al., 2001; Sharma and Subramanian, 2008; Jha et al., 2009; Rengarajan et al., 2009; Gupta et al., 2011; Mehto and Chakrapani, 2013; Hartmann et al., 2014a; Moon et al., 2014); 6 (Pokrovsky et al., 2005; Prokushkin et al., 2011); 7–11, 29 (This work; Li and Long, 2014); 12, 30 (Han and Huh, 2009); 15 (Lyons et al., 2005; Blazina and Sharma, 2013); 16, 34 (Schopka and Derry, 2012); 17 (Dessert et al., 2003); 18 (Herrera and Custodio, 2008); 21 (Benedetti et al., 1994); 22 (Van der Weijden and Pacheco, 2003; Prada et al., 2005); 23 (Benedetti et al., 2003); 24 (Aiuppa et al., 2000; Brusca et al., 2001); 25 (Balagizi et al., 2015); 26 (Louvat and Allègre, 1997); 27 (Aldrian et al., 2008); 28 (Schopka et al., 2011); 32 (Dessert et al., 2009); 33 (Goldsmith et al., 2008, 2010; Blazina and Sharma, 2013); 36 (Freire et al., 2013); 37 (Gislason et al., 1996; Eiriksdottir et al., 2008; Louvat et al., 2008).

Table 2
Results of simple correlations using the best values in Table 1 and Monte Carlo statistics that incorporate uncertainties.

Form of equation[a]	$K_{CO_2} = e^a e^{-b\times 1000/(MAT+273)/R}$ [b]			$K_{CO_2} = e^a RUN^b$			$RUN = e^a e^{bMAT}$			$C = e^a e^{bMAT}$			$C = e^a RUN^{-b}$		
Physical bases	Arrhenius form			Prediction of Eq. (1)			Clausius–Clapeyron relationship			Eq. (1)			Dilution effect		
Data plot	Fig. 1(a)			Fig. 1(b)			Fig. 3			Fig. 4(a)			Fig. 4(b)		
	All data	AVFs	IVFs	All data	AVFs	IVFs	All data	AVFs	IVFs	All data	AVFs	IVFs	All data	AVFs	IVFs
p value															
Simple correlation	$<10^{-3}$	0.054	$<10^{-8}$	$<10^{-5}$	0.02	0.01	0.01	0.14	0.02	0.08	0.25	0.16	0.25	0.78	$<10^{-2}$
Monte Carlo statistics	$<10^{-3}$	0.69	$<10^{-3}$	$<10^{-2}$	0.35	0.16	0.30	0.99	0.08	0.88	1.00	0.99	0.96	1.00	0.08
r^2															
Simple correlation	0.31	0.26	0.85	0.44	0.36	0.29	0.17	0.16	0.26	0.09	0.10	0.10	0.04	0.01	0.36
Monte Carlo statistics	0.28	0.23	0.75	0.38	0.30	0.25	0.13	0.13	0.24	0.07	0.08	0.09	0.03	0.02	0.30
a															
Simple correlation	15.6	13.9	17.0	−5.63	−5.84	−3.71	6.06	6.63	5.67	6.76	7.05	6.55	8.19	7.97	10.1
Monte Carlo statistics	15.3	13.5	16.7	−5.20	−5.01	−3.53	6.04	6.62	5.65	6.74	7.05	6.53	8.13	8.01	9.87
b															
Simple correlation	37.8	32.0	42.2	0.82	0.91	0.46	0.035	0.025	0.041	0.023	0.024	0.022	0.18	0.09	0.54
Monte Carlo statistics	37.0	31.0	41.6	0.75	0.78	0.43	0.032	0.023	0.041	0.022	0.021	0.022	0.18	0.10	0.50

[a] a, b are fit parameters determined in each regression.
[b] R is gas constant of 8.314 J/K/mol.

of the relationships used). In each case, correlations were analyzed using a Monte Carlo method, in order to account for and propagate uncertainties. All functional relationships were transformed to linear form (e.g., $y = ax^b$ to $\ln(y) = b\ln(x) + \ln(a)$; $y = ae^{bx}$ to $\ln(y) = \ln(b)x + \ln(a)$). A hypothetical dataset was generated from observed x and y values by adding random errors following normal distributions defined by observed σ_m (Table 1). The hypothetical dataset was then log-transformed and fit to the linear-form regression model. Regression coefficients (a and b), r^2, and p values (p_{MC}) were recorded for every simulation. The simulation was repeated 100 000 times. The mean and standard deviation of the regression coefficients and r^2 from the 100 000 simulations were calculated as the final regression results. The significance of the final regression results was judged by the fraction (p) of insignificant correlations ($p_{MC} >= 0.05$) among the 100 000 simulations. A p-value <0.05, i.e., when more than 95% of the simulated correlations were significant, means that the correlation between the observed x and y values are significant at the 95% confidence level considering the uncertainty in the data.

The data analysis also involved tests of uniform distribution and evaluations of equal medians. To test for uniform distributions, Kolmogorov–Smirnov statistics were used. To check whether the medians of two uniformly distributed datasets are equal, a Wilcoxon rank sum test was used.

Finally, a Monte Carlo simulation was used to test if the overall correlation between runoff and K_{CO_2} (Fig. 2(b)) is affected by (1) the high runoff of AVFs and (2) the cross-correlation between runoff and K_{CO_2} (since K_{CO_2} is calculated by multiplying the concentration of DIC with runoff). First, to test for the role of the different runoff in AVFs versus IVFs, hypothetical runoff and K_{CO_2} values for each basalt region were randomly generated according to the observed distribution of runoff and K_{CO_2} in the compiled AVFs and IVFs. Bicarbonate concentrations of these hypothetical catchments were calculated from the generated K_{CO_2} and runoff. To consider the effect from possible cross-correlation of K_{CO_2} and runoff, the runoff of each hypothetical catchment was modified by adding a normally distributed random value with a coefficient of variation of 20±14% (mean ± standard deviation) and 19±18% for AVFs and IVFs, respectively. A new K_{CO_2} value for each hypothetical catchment was calculated from the bicarbonate concentration and modified runoff. Finally, correlation parameters between the new K_{CO_2} and runoff were calculated across all of the catchments. The simulation was run 100 000 times and average correlation results of the simulation were calculated.

3. Results

In total, data from 37 basaltic regions (22 IVFs and 15 AVFs) were compiled (Table 1), covering most of the basaltic fields of the world (Fig. 1). Runoff and MAT in the dataset range from 74 to 2120 mm/yr and from −9 to 27 °C, respectively (Fig. 3). The number of basaltic fields and the variation of MAT and runoff significantly expand the prior compilation of Dessert et al. (2003). No statistically significant Clausius–Clapeyron type relationship (Table 2) between temperature and precipitation (Allen and Ingram, 2002) can be found between MAT and runoff at the 95% confidence level, either for all data or for AVFs and IVFs alone. The AVFs and IVFs show similar uniform distributions of MAT and logarithm of runoff. The median MAT of AVFs is statistically indistinguishable from that of IVFs within uncertainty. However, the AVFs have statistically higher runoff than the IVFs (6.91 ± 0.17 vs. 6.13 ± 0.18 in the mean ± standard error of the mean for natural logarithm value in units of mm/yr).

K_{CO_2} is positively related to MAT for all data in Arrhenius form (Table 2; Fig. 2(a); $r^2 = 0.28$; $p < 10^{-3}$). However, no such simple correlation can be observed for AVFs only ($r^2 = 0.23$; $p = 0.69$).

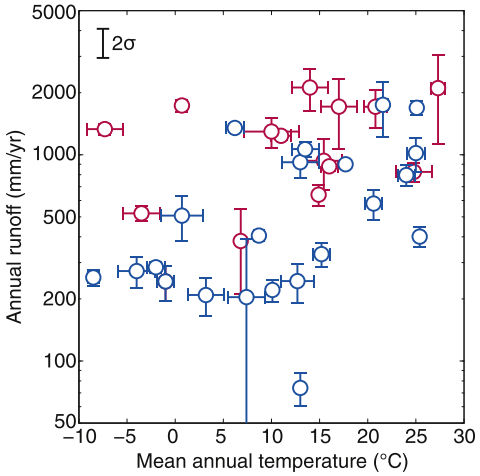

Fig. 3. Range of annual runoff and mean annual temperature for the compiled basaltic fields. Error bars show 2× standard deviation of the mean ($2\sigma_m$). Labels are the same as those in Fig. 1.

Thus, the overall MAT-K_{CO_2} correlation is defined primarily by the IVFs (Fig. 2(a); $r^2 = 0.75$; $p < 10^{-3}$). For a given temperature, the K_{CO_2} of AVFs is much higher than that of the IVFs. On average, the K_{CO_2} of AVFs (2.23×10^6 mol/km^2/yr) is four times that of the IVFs, at 0.52×10^6 mol/km^2/yr (the equal median hypothesis was rejected by the Wilcoxon rank sum test).

There is a weak correlation in the power-law relation (Table 2) between runoff and K_{CO_2} for all data ($r^2 = 0.38$; $p < 0.01$), with a power-law exponent of 0.75 ± 0.09 (mean ± standard deviation). When ignoring uncertainty in the observations, i.e., using only best estimate values in Table 1 rather than the Monte Carlo analysis that incorporates uncertainties, the implied runoff–K_{CO_2} correlation is stronger ($r^2 = 0.44$; $p < 10^{-5}$; power-law exponent 0.82 ± 0.16). There is no significant runoff–K_{CO_2} correlation if AVFs ($r^2 = 0.30$; $p = 0.35$) and IVFs ($r^2 = 0.2$; $p = 0.16$) are considered separately (Fig. 2(b)). These correlations do become significant ($p = 0.04$) when excluding outliers for IVFs (data #13 from South Australia) but not for AVFs ($p = 0.08$, #24 from Mt. Etna). The runoff–K_{CO_2} correlations would be significant ($p < 0.05$) for both AVFs and IVFs if not considering data uncertainties. No better correlation between runoff and K_{CO_2} is found by using other functions, e.g. an exponential form (Maher, 2010, 2011).

DIC concentration shows no correlation with MAT following the form proposed by Dessert et al. (2003) or with runoff in the form of a simple dilution relationship (Table 2), either for all data or if AVFs and IVFs are considered separately (Fig. 4).

4. Discussion

4.1. Compatibility with the Dessert et al. (2003) model

We first examine compatibility of the new data compilation with the model of Dessert et al. (2003), i.e., Eq. (1). This model largely depends on the temperature dependence of bicarbonate concentration (C), where $C = c_2 \exp(c_1 \times \text{MAT})$. The previous dataset of ten basaltic catchments was described well by this relationship ($r^2 = 0.71$) with values of 0.0638 and 324 for c_1 and c_2, respectively (Dessert et al., 2003). In contrast, the absence of a significant concentration–MAT correlation in the new data compilation, either for all data or for AVFs or IVFs considered separately (Fig. 4(a)), is not consistent with the model of Dessert et al. (2003). The difference between this study and that of Dessert et al. (2003) could potentially relate to either: (1) updating values from the original dataset due to different strategies of data collection and the addition of new observations from these

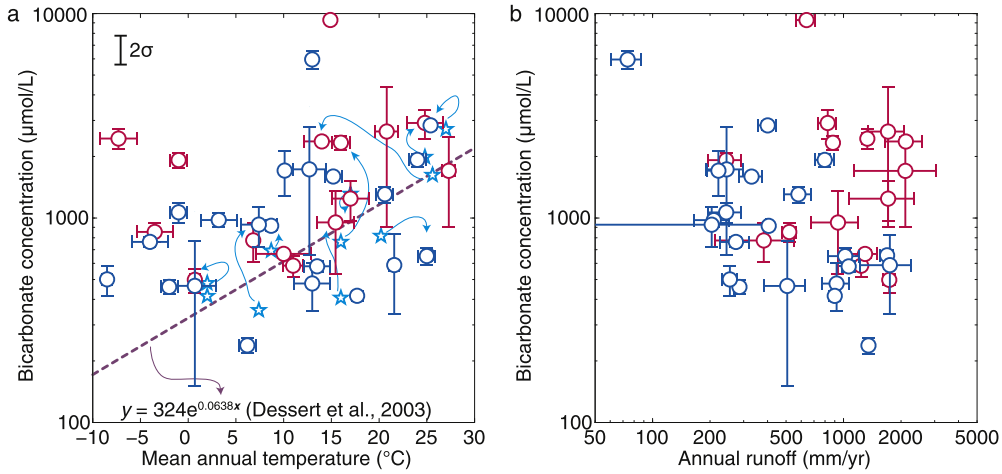

Fig. 4. Cross-plots between concentration of bicarbonate and climate factors. (a) Cross-plot between temperature and concentration of bicarbonate. No significant correlation is found for all data considered together, or for the active and inactive volcanic fields separately. Dashed line is the correlation based on the 10 basaltic fields compiled by Dessert et al. (2003) (open cyan stars; note that there are two points for Iceland). The arrows connect the original and updated data for the same basaltic fields. The updated data for these ten basaltic fields still give significant correlation ($y = 593e^{0.0499x}$; $r^2 = 0.44$; $p = 0.026$). (b) Cross-plot between annual runoff and concentration of bicarbonate. No correlation can be found for all data considered together, or for the active and inactive volcanic fields separately. Error bars show 2× standard deviation of the mean ($2\sigma_m$). Labels are the same as those in Fig. 1. (For interpretation of the references to color in this figure legend, the reader is referred to the web version of this article.)

previously-considered regions (refer to the supplementary material for details); (2) changing the regression technique, in this study considering uncertainties in MAT and concentration; or (3) expanding the dataset to include other regions. Using the original regression technique and updated data from the ten original catchments used by Dessert et al. (2003) still gives a significant concentration-MAT correlation ($r^2 = 0.46$; $p = 0.03$; Fig. 4(a)), with values of 0.0484 and 572 for c_1 and c_2, respectively. On the other hand, the original regression technique does not yield a significant correlation with the new data, either for all data or for AVFs and IVFs separately. Thus, the previously observed correlation between MAT and DIC concentration can be attributed to the limited scope of the previous dataset, as compared to the expanded set of sites in our new compilation.

Eq. (1) also predicts a power-law relationship between K_{CO_2} and runoff with an exponent of 1. The positive correlation between K_{CO_2} and runoff for all data in our compilation (power-law exponent 0.75 ± 0.09; Fig. 4(b)) is marginally consistent with such a prediction. However, we cannot confidently determine whether the positive correlation reflects a control of runoff on basalt weathering because the same correlation is absent when either AVFs or IVFs are considered separately.

The apparent correlation between K_{CO_2} and runoff for the whole dataset could be related to the coincidence of high weathering rate and higher runoff of active volcanic fields. Many active volcanoes are located near the oceans (Fig. 1) and have high topography, a combination that contributes to their higher runoff (Gaillardet et al., 2011). The coincident high weathering rates may be partly related to the high runoff but may also be affected by several other factors (discussed below in Section 4.3). The correlation between K_{CO_2} and runoff could also be related to the cross-correlation between these parameters. Calculated CO_2 consumption includes a runoff term, so uncertainties in runoff values could generate an apparent correlation because over or under estimation of runoff would introduce the same degree of over or under estimation of the calculated K_{CO_2}. Monte Carlo analysis suggests that the high runoff of AVFs and the cross-correlation between runoff and K_{CO_2} together would yield an estimated relationship between K_{CO_2} and runoff defined by $K_{CO_2} = e^{-3.19\pm1.20} RUN^{0.44\pm0.19}$ ($r^2 = 0.17 \pm 0.12$). This predicted relationship is close to the observed correlation within error (Fig. 2(b)). Neither the effect of cross-correlation nor the high runoff associated with AVFs can on its own produce the observed correlation. Thus, based on the present dataset, we cannot conclusively identify whether or not there is a significant role for runoff in determining basalt-weathering rates.

4.2. Temperature control of IVF weathering

A general kinetic law has been proposed for the dependence of mineral weathering rate on temperature, the $\alpha^3_{H^+}/\alpha_{Al^{+3}}$ activity of the aqueous solution, and the saturation state with respect to the dissolving phase (Lasaga et al., 1994; Oelkers and Gislason, 2001; Gislason and Oelkers, 2003; Eiriksdottir et al., 2013):

$$K_{CO_2} = sAe^{\frac{-E_a}{RT}} \left(\frac{\alpha^3_{H^+}}{\alpha_{Al^{+3}}}\right)^{\frac{1}{3}} \left(1 - e^{\frac{\Delta G_r}{RT}}\right) \quad (2)$$

where s ($m^2/K\,m^2$) is the normalized reactive surface area, A the pre-exponential constant (mol/m^2/yr) that reflects weathering reactivity, E_a (J/mol) the apparent activation energy of the Arrhenius term, R (8.314 J/mol/K) the universal gas constant, T (K) the MAT in absolute temperature, and ΔG_r (J/mol) the Gibbs free energy of the weathering reaction. $\alpha^3_{H^+}/\alpha_{Al^{+3}}$, which controls exchange reaction between H^+ and Al in the silicate structure and thus regulates Al release (Oelkers and Gislason, 2001; Gislason and Oelkers, 2003), represents the increase in dissolution rate with more acidic protons, e.g., those associated with dissolved CO_2 in the form of carbonic acid or organic acids.

It is likely that the exponential relationship between MAT and K_{CO_2} for IVFs reflects an Arrhenius relationship. The implied E_a, 41.6 ± 3.2 kJ/mol (mean ± standard deviation) (Fig. 2(a)), is very close to values obtained from laboratory dissolution of diopside (41 kJ/mol, Knauss et al., 1993) and labradorite (42 kJ/mol, Carroll and Knauss, 2005), the two most common minerals in basalts. However, the value of E_a is higher than has been observed experimentally for the dissolution of volcanic glass (25.5 kJ/mol; Gislason and Oelkers, 2003).

The strong correlation between MAT and K_{CO_2} for IVFs (Fig. 2(a)) suggests that temperature is a dominant predictor of IVF basalt weathering rate at the global scale. The K_{CO_2} predictions based on temperature, i.e., Eq. (2), yield root mean square of relative deviation (RMSRD) between observed and predicted values of 28% for IVFs, which is similar to the mean CV of K_{CO_2} estimated

for the IVFs (19 ± 9%). In contrast, the K_{CO_2} predictions made by runoff (Fig. 2(b); $K_{CO_2} = e^{-5.20\pm0.57} RUN^{0.75\pm0.09}$) yield much higher RMSRD of 88%, 56%, and 104% for all data, AVFs, and IVFs, respectively. Predictions of K_{CO_2} based on the combination of temperature and runoff yield RMSRD of 73%, 72%, and 28% for all data, AVFs, and IVFs, respectively (using multiple regression technique in form of $K_{CO_2} = RUN^a \times c_2 \times e^{c1 \times MAT}$). The smaller RMSRDs of this prediction compared to those made by runoff alone is mainly contributed by the correlation between MAT and K_{CO_2}. On the other hand, considering runoff together with MAT does not improve prediction relative to considering MAT alone for IVFs.

One important question arising from this compilation is why there is not a more evident role for runoff in determining weathering fluxes from basaltic catchments. Runoff influences weathering mainly by increasing the water–rock ratio, i.e., the reactive wet surface s in Eq. (2), and/or by driving the weathering reaction further from equilibrium by diluting the weathering solution, affecting the $(1 - \Delta G_r/RT)$ term in Eq. (2) (Eiriksdottir et al., 2013; Maher and Chamberlain, 2014). The saturation state of rivers in Iceland and Sao Miguel suggest that weathering of basalt might be relatively far from chemical equilibrium with respect to rock forming minerals, i.e., with very negative ΔG_r (Pogge von Strandmann et al., 2006, 2010; Eiriksdottir et al., 2013). If this is the case, the dilution effect of runoff would be minor because the dissolution rate of minerals under conditions far from equilibrium remains at a plateau value that is not sensitive to changing degree of undersaturation (Lasaga et al., 1994; Maher, 2011).

4.3. Complexities in active volcanic fields

We suggest that temperature does not predict the K_{CO_2} of AVFs due to the other factors that influence the observed weathering flux. Several mechanisms may explain the high and variable flux of DIC observed in AVFs, and the lack of correlation between MAT and K_{CO2}. As discussed above, the focusing of orographic rainfall and thus high runoff may play some role (e.g., Gaillardet et al., 2011), though this role is difficult to separate from other factors on the basis of our compilation. Young volcanic rocks, characterized by highly porous lava flows and pyroclastic deposits, may have greater reactive surface area, i.e., the term s in Eq. (2). In addition, the shielding effect due to the development of soil probably reduces the effective reactive surface area in aged volcanic fields (Bluth and Kump, 1994; Hartmann et al., 2014b). Uncrystallized volcanic glass may also have higher weathering reactivity, i.e., higher A value in Eq. (2), compared to crystallized basaltic rocks (Gislason et al., 1996, 2009). It is also possible that the dominant secondary minerals, and the resulting effects on $\alpha^3_{H^+}/\alpha_{Al^{+3}}$ activity ratio, may differ between active and inactive volcanic regions. CO_2-rich magmatic fluids may also contribute directly to observed alkalinity fluxes from active volcanic areas. It has been shown that the contribution of CO_2-rich magmatic fluids may contribute a relevant fraction of observed alkalinity fluxes from active volcanic areas (Aiuppa et al., 2000; Rad et al., 2007; Gaillardet et al., 2011; Rivé et al., 2013; Henchiri et al., 2014), as can deep high temperature weathering (Louvat and Allègre, 1997). In addition, it is also possible that younger basalts have more hydrothermal calcite that might be subjected to fast weathering (Jacobson et al., 2015).

The above factors may be related to eruption age, helping explain why weathering rates of volcanic systems decrease dramatically within approximately the first one million years after eruption and in some cases even faster, eventually reaching a plateau (Vitousek et al., 1997; Louvat et al., 2008; Rad et al., 2013; Freire et al., 2014). It is difficult to evaluate the average eruption age of the volcanic fields in our data compilation due to the dynamic eruption history. Nonetheless, it is clear that Mt. Cameroon, Mt. Etna, Mt. Virunga, and Mt. Changbaishan (Tianchi Lake), where volcanic activities were observed in recent decades, are among the youngest volcanic fields compiled. These regions are characterized by very high K_{CO_2} and the largest deviation from the general correlation between K_{CO_2} and MAT (Fig. 2(a)), consistent with an influence of AVF age on K_{CO_2}.

Ground water discharge may introduce additional variability in the observed K_{CO_2} in AVFs. The young geomorphic setting of AVFs is generally characterized high groundwater discharge because drainage systems have not yet been fully developed (Jefferson et al., 2010). Except in a few specific cases (e.g., Schopka and Derry, 2012), the flux of weathering products carried via groundwater discharge has not been well constrained or even considered.

4.4. Implication for long-term carbon cycle

Basaltic rocks are estimated to cover only ~3.5% to ~5% of the global land surface (Dessert et al., 2003; Hartmann and Moosdorf, 2012) but contribute a more significant 30% of the CO_2 consumed by silicate weathering globally (Gaillardet et al., 1999; Dessert et al., 2003). The approximately three times higher K_{CO_2} from AVFs compared to IVFs supports the notion that basalt weathering may have influenced the carbon cycle during time periods in the geologic past characterized by large, active volcanic systems (Schaller et al., 2012; Mills et al., 2014).

The finding of strong temperature influence on basalt weathering of IVFs implies that basalt weathering may also have played a central role in restoring balance in the geologic carbon cycle following perturbation (e.g., Dessert et al., 2001; Donnadieu et al., 2006; Goddéris et al., 2014). An example of the role of varying basalt-weathering reactivity might be found in the history of the Cenozoic. Tectonic uplift during the Cenozoic may have changed the carbon cycle fluxes associated with continental silicate weathering and the recycling of organic carbon (Raymo et al., 1988; Goddéris and François, 1995; France-Lanord and Derry, 1997; Wallmann, 2001; Misra and Froelich, 2012; Torres et al., 2014). Mass balance modeling of marine isotopic records shows that the associated perturbations in the carbon cycle could have been balanced by a progressive decrease in basalt weathering by ~37% since the late Cretaceous (Li and Elderfield, 2013). This change would imply a global cooling of 8 °C using an average activation energy of 41.6 kJ/mol (as we find for IVFs in the present day) and assuming no substantial changes in exposure area and geographic distribution of basaltic rocks (cf. Kent and Muttoni, 2013; Mills et al., 2014). Such magnitude of cooling is consistent with reconstruction of climate change since the Cretaceous based on other proxies (Lear et al., 2000; Norris et al., 2013).

5. Conclusion

A new data compilation covering 37 regions worldwide allows us to revisit the influence of climatic parameters on basalt weathering rates, and thus to better understand stabilizing feedbacks in the planetary carbon cycle. We find a strong relationship between mean annual temperature and rates of CO_2 consumption for inactive volcanic fields. This temperature relationship is not evident when also including data from active volcanic fields, a difference that we attribute to a range of complicating factors in active volcanic regions, including the reactivity of recently erupted basalt and hydrothermal reactions that may not depend directly on climate. The new data do not demonstrate a clear role for runoff as an independent controlling variable for CO_2 consumption during basalt weathering, but nor do the data conclusively rule out an effect of runoff. A stronger connection between runoff and CO_2 consumption would be (erroneously) inferred from data analysis not accounting for observational uncertainties, emphasizing the

importance of considering uncertainties when assessing such relationships.

Relative to their coverage of land area, weathering of basalt contributes a disproportionate share of the silicate-derived alkalinity flux delivered to the oceans, so climate sensitivity of CO_2 consumption during basalt weathering can be globally important even if basalts account for a modest fraction of the terrestrial surface. Strong dependence of CO_2 consumption during the weathering of basalts on temperature thus provides a viable feedback mechanism between CO_2 and climate, consistent with the concept of a stabilizing chemical weathering thermostat.

Acknowledgements

Ken Ferrier and three anonymous reviewers are thanked for their constructive comments that helped improve the manuscript. We thank Pascale Louvat for providing the original data from her work and translating the French data tables of Meybeck (1986). Support for this work comes from National Natural Science Foundation of China funding (grant Nos. 41173105, 41422205, and 41321062). Jens Hartmann was supported by the German Science Foundation (DFG-project HA4472/6-1 and the Cluster of Excellence 'CliSAP', EXC177, Universität Hamburg).

Appendix A. Supplementary material

Supplementary material related to this article can be found online at http://dx.doi.org/10.1016/j.epsl.2016.03.015.

References

Aiuppa, A., et al., 2000. Mobility and fluxes of major, minor and trace metals during basalt weathering and groundwater transport at Mt. Etna volcano (Sicily). Geochim. Cosmochim. Acta 64 (11), 1827–1841.

Aldrian, E., et al., 2008. Spatial and seasonal dynamics of riverine carbon fluxes of the Brantas catchment in East Java. J. Geophys. Res., Biogeosci. 113 (G3), G03029.

Allen, M.R., Ingram, W.J., 2002. Constraints on future changes in climate and the hydrologic cycle. Nature 419 (6903), 224–232.

Amiotte-Suchet, P., Probst, J.L., 1995. A global model for present-day atmospheric/soil CO_2 consumption by chemical erosion of continental rocks (GEM-CO_2). Tellus B 47 (1–2), 273–280.

Arvidson, R.S., Mackenzie, F.T., Guidry, M., 2006. MAGic: a Phanerozoic model for the geochemical cycling of major rock-forming components. Am. J. Sci. 306 (3), 135–190.

Balagizi, C.M., et al., 2015. River geochemistry, chemical weathering, and atmospheric CO_2 consumption rates in the Virunga Volcanic Province (East Africa). Geochem. Geophys. Geosyst. 16 (8), 2637–2660.

Benedetti, M.F., et al., 2003. Chemical weathering of basaltic lava flows undergoing extreme climatic conditions: the water geochemistry record. Chem. Geol. 201 (1–2), 1–17.

Benedetti, M.F., Menard, O., Noack, Y., Carvalho, A., Nahon, D., 1994. Water–rock interactions in tropical catchments: field rates of weathering and biomass impact. Chem. Geol. 118 (1–4), 203–220.

Berner, R.A., Caldeira, K., 1997. The need for mass balance and feedback in the geochemical carbon cycle. Geology 25 (10), 955–956.

Berner, R.A., Kothavala, Z., 2001. GEOCARB III: a revised model of atmospheric CO_2 over Phanerozoic time. Am. J. Sci. 301 (2), 182–204.

Berner, R.A., Lasaga, A.C., Garrels, R.M., 1983. The carbonate–silicate geochemical cycle and its effect on atmospheric carbon dioxide over the past 100 million years. Am. J. Sci. 283 (7), 641–683.

Blazina, T., Sharma, M., 2013. Chemical weathering on the North Island of New Zealand: CO_2 consumption and fluxes of Sr and Os. Geochem. Geophys. Geosyst. 14 (9), 3600–3615.

Bluth, G.J.S., Kump, L.R., 1994. Lithologic and climatologic controls of river chemistry. Geochim. Cosmochim. Acta 58 (10), 2341–2359.

Brusca, L., et al., 2001. Geochemical mapping of magmatic gas–water–rock interactions in the aquifer of Mount Etna volcano. J. Volcanol. Geotherm. Res. 108 (1–4), 199–218.

Capo, R.C., Whipkey, C.E., Blachère, J.R., Chadwick, O.A., 2000. Pedogenic origin of dolomite in a basaltic weathering profile, Kohala peninsula, Hawaii. Geology 28 (3), 271–274.

Carroll, S.A., Knauss, K.G., 2005. Dependence of labradorite dissolution kinetics on CO_2(aq), Al(aq), and temperature. Chem. Geol. 217 (3–4), 213–225.

Conley, D.J., 2002. Terrestrial ecosystems and the global biogeochemical silica cycle. Glob. Biogeochem. Cycles 16 (4), 1121.

Das, A., Krishnaswami, S., Sarin, M.M., Pande, K., 2005. Chemical weathering in the Krishna Basin and Western Ghats of the Deccan Traps, India: rates of basalt weathering and their controls. Geochim. Cosmochim. Acta 69 (8), 2067–2084.

Derry, L.A., Kurtz, A.C., Ziegler, K., Chadwick, O.A., 2005. Biological control of terrestrial silica cycling and export fluxes to watersheds. Nature 433 (7027), 728–731.

Dessert, C., et al., 2001. Erosion of Deccan Traps determined by river geochemistry: impact on the global climate and the $^{87}Sr/^{86}Sr$ ratio of seawater. Earth Planet. Sci. Lett. 188 (3–4), 459–474.

Dessert, C., Dupré, B., Gaillardet, J., François, L.M., Allègre, C.J., 2003. Basalt weathering laws and the impact of basalt weathering on the global carbon cycle. Chem. Geol. 202 (3–4), 257–273.

Dessert, C., Gaillardet, J., Dupre, B., Schott, J., Pokrovsky, O.S., 2009. Fluxes of high- versus low-temperature water–rock interactions in aerial volcanic areas: example from the Kamchatka Peninsula, Russia. Geochim. Cosmochim. Acta 73 (1), 148–169.

Dixon, J.L., Hartshorn, A.S., Heimsath, A.M., DiBiase, R.A., Whipple, K.X., 2012. Chemical weathering response to tectonic forcing: a soils perspective from the San Gabriel Mountains, California. Earth Planet. Sci. Lett. 323–324, 40–49.

Donnadieu, Y., et al., 2006. A GEOCLIM simulation of climatic and biogeochemical consequences of Pangea breakup. Geochem. Geophys. Geosyst. 7 (11), Q11019.

Eiriksdottir, E.S., Gislason, S.R., Oelkers, E.H., 2013. Does temperature or runoff control the feedback between chemical denudation and climate? Insights from NE Iceland. Geochim. Cosmochim. Acta 107 (0), 65–81.

Eiriksdottir, E.S., Louvat, P., Gislason, S.R., Óskarsson, N., Hardardóttir, J., 2008. Temporal variation of chemical and mechanical weathering in NE Iceland: evaluation of a steady-state model of erosion. Earth Planet. Sci. Lett. 272 (1–2), 78–88.

Evans, M.J., Derry, L.A., Anderson, S.P., France-Lanord, C., 2001. Hydrothermal source of radiogenic Sr to Himalayan rivers. Geology 29 (9), 803–806.

Evans, M.J., Derry, L.A., France-Lanord, C., 2004. Geothermal fluxes of alkalinity in the Narayani river system of central Nepal. Geochem. Geophys. Geosyst. 5.

Fekete, B.M., Vorosmarty, C.J., Grabs, W., 2002. High-resolution fields of global runoff combining observed river discharge and simulated water balances. Glob. Biogeochem. Cycles 16 (3).

Ferrier, K.L., Kirchner, J.W., 2008. Effects of physical erosion on chemical denudation rates: a numerical modeling study of soil-mantled hillslopes. Earth Planet. Sci. Lett. 272 (3–4), 591–599.

Ferrier, K.L., Kirchner, J.W., Finkel, R.C., 2012. Weak influences of climate and mineral supply rates on chemical erosion rates: measurements along two altitudinal transects in the Idaho Batholith. J. Geophys. Res., Earth Surf. 117, 21.

France-Lanord, C., Derry, L.A., 1997. Organic carbon burial forcing of the carbon cycle from Himalayan erosion. Nature 390 (6655), 65–67.

Freire, P., Andrade, C., Coutinho, R., Cruz, J.V., 2013. Fluvial geochemistry in São Miguel Island (Azores, Portugal): source and fluxes of inorganic solutes in an active volcanic environment. Sci. Total Environ. 454–455 (0), 154–169.

Freire, P., Andrade, C., Coutinho, R., Cruz, J.V., 2014. Spring geochemistry in an active volcanic environment (São Miguel, Azores): source and fluxes of inorganic solutes. Sci. Total Environ. 466–467 (0), 475–489.

Gaillardet, J., Dupré, B., Louvat, P., Allègre, C.J., 1999. Global silicate weathering and CO_2 consumption rates deduced from the chemistry of large rivers. Chem. Geol. 159 (1–4), 3–30.

Gaillardet, J., Millot, R., Dupré, B., 2003. Chemical denudation rates of the western Canadian orogenic belt: the Stikine terrane. Chem. Geol. 201 (3–4), 257–279.

Gaillardet, J., et al., 2011. Orography-driven chemical denudation in the Lesser Antilles: evidence for a new feed-back mechanism stabilizing atmospheric CO_2. Am. J. Sci. 311 (10), 851–894.

Gislason, S.R., Arnorsson, S., Armannsson, H., 1996. Chemical weathering of basalt in Southwest Iceland; effects of runoff, age of rocks and vegetative/glacial cover. Am. J. Sci. 296 (8), 837–907.

Gislason, S.R., Oelkers, E.H., 2003. Mechanism, rates, and consequences of basaltic glass dissolution: II. An experimental study of the dissolution rates of basaltic glass as a function of pH and temperature. Geochim. Cosmochim. Acta 67 (20), 3817–3832.

Gislason, S.R., et al., 2009. Direct evidence of the feedback between climate and weathering. Earth Planet. Sci. Lett. 277 (1–2), 213–222.

Goddéris, Y., Donnadieu, Y., Le Hir, G., Lefebvre, V., Nardin, E., 2014. The role of palaeogeography in the Phanerozoic history of atmospheric CO_2 and climate. Earth-Sci. Rev. 128, 122–138.

Goddéris, Y., François, L.M., 1995. The Cenozoic evolution of the strontium and carbon cycles: relative importance of continental erosion and mantle exchanges. Chem. Geol. 126 (2), 169–190.

Goldsmith, S.T., et al., 2010. Stream geochemistry, chemical weathering and CO_2 consumption potential of andesitic terrains, Dominica, Lesser Antilles. Geochim. Cosmochim. Acta 74 (1), 85–103.

Goldsmith, S.T., Carey, A.E., Lyons, W.B., Hicks, D.M., 2008. Geochemical fluxes and weathering of volcanic terrains on high standing islands: Taranaki and Manawatu–Wanganui regions of New Zealand. Geochim. Cosmochim. Acta 72 (9), 2248–2267.

Gupta, H., Chakrapani, G.J., Selvaraj, K., Kao, S.-J., 2011. The fluvial geochemistry, contributions of silicate, carbonate and saline-alkaline components to chemical weathering flux and controlling parameters: Narmada River (Deccan Traps), India. Geochim. Cosmochim. Acta 75 (3), 800–824.
Han, Y., Huh, Y., 2009. A geochemical reconnaissance of the Duman (Tumen) River and the hot springs of Mt. Baekdu (Changbai): weathering of volcanic rocks in mid-latitude setting. Chem. Geol. 264 (1–4), 162–172.
Harrison, J.A., Frings, P.J., Beusen, A.H.W., Conley, D.J., McCrackin, M.L., 2012. Global importance, patterns, and controls of dissolved silica retention in lakes and reservoirs. Glob. Biogeochem. Cycles 26 (2), GB2037.
Hartmann, J., 2009. Bicarbonate-fluxes and CO_2-consumption by chemical weathering on the Japanese Archipelago — application of a multi-lithological model framework. Chem. Geol. 265 (3–4), 237–271.
Hartmann, J., Lauerwald, R., Moosdorf, N., 2014a. A brief overview of the GLObal RIver Chemistry Database, GLORICH. Proc. Earth Planet. Sci. 10 (0), 23–27.
Hartmann, J., Moosdorf, N., 2012. The new global lithological map database GLiM: a representation of rock properties at the Earth surface. Geochem. Geophys. Geosyst. 13 (12), Q12004.
Hartmann, J., Moosdorf, N., Lauerwald, R., Hinderer, M., West, A.J., 2014b. Global chemical weathering and associated P-release — the role of lithology, temperature and soil properties. Chem. Geol. 363 (0), 145–163.
Henchiri, S., et al., 2014. The influence of hydrothermal activity on the Li isotopic signature of rivers draining volcanic areas. Proc. Earth Planet. Sci. 10 (0), 223–230.
Herrera, C., Custodio, E., 2008. Conceptual hydrogeological model of volcanic Easter Island (Chile) after chemical and isotopic surveys. Hydrogeol. J. 16 (7), 1329–1348.
Hijmans, R.J., Cameron, S.E., Parra, J.L., Jones, P.G., Jarvis, A., 2005. Very high resolution interpolated climate surfaces for global land areas. Int. J. Climatol. 25 (15), 1965–1978.
Jacobson, A.D., Grace Andrews, M., Lehn, G.O., Holmden, C., 2015. Silicate versus carbonate weathering in Iceland: new insights from Ca isotopes. Earth Planet. Sci. Lett. 416 (0), 132–142.
Jefferson, A., Grant, G.E., Lewis, S.L., Lancaster, S.T., 2010. Coevolution of hydrology and topography on a basalt landscape in the Oregon Cascade Range, USA. Earth Surf. Process. Landf. 35 (7), 803–816.
Jha, P.K., Tiwari, J., Singh, U.K., Kumar, M., Subramanian, V., 2009. Chemical weathering and associated CO_2 consumption in the Godavari river basin, India. Chem. Geol. 264 (1–4), 364–374.
Kelemen, P.B., Matter, J., 2008. In situ carbonation of peridotite for CO_2 storage. Proc. Natl. Acad. Sci. USA 105 (45), 17295–17300.
Kent, D.V., Muttoni, G., 2013. Modulation of Late Cretaceous and Cenozoic climate by variable drawdown of atmospheric pCO_2 from weathering of basaltic provinces on continents drifting through the equatorial humid belt. Clim. Past 9 (2), 525–546.
Knauss, K.G., Nguyen, S.N., Weed, H.C., 1993. Diopside dissolution kinetics as a function of pH, CO_2, temperature, and time. Geochim. Cosmochim. Acta 57 (2), 285–294.
Kump, L.R., Brantley, S.L., Arthur, M.A., 2000. Chemical, weathering, atmospheric CO_2, and climate. Annu. Rev. Earth Planet. Sci. 28, 611–667.
Lasaga, A.C., Soler, J.M., Ganor, J., Burch, T.E., Nagy, K.L., 1994. Chemical weathering rate laws and global geochemical cycles. Geochim. Cosmochim. Acta 58 (10), 2361–2386.
Lear, C.H., Elderfield, H., Wilson, P.A., 2000. Cenozoic deep-sea temperatures and global ice volumes from Mg/Ca in benthic foraminiferal calcite. Science 287 (5451), 269–272.
Li, G., Elderfield, H., 2013. Evolution of carbon cycle over the past 100 million years. Geochim. Cosmochim. Acta 103 (0), 11–25.
Li, G., Long, X., 2014. Weathering of Chinese basaltic fields. Proc. Earth Planet. Sci. 10 (0), 69–72.
Lloret, E., et al., 2011. Comparison of dissolved inorganic and organic carbon yields and fluxes in the watersheds of tropical volcanic islands, examples from Guadeloupe (French West Indies). Chem. Geol. 280 (1–2), 65–78.
Lohse, K.A., Dietrich, W.E., 2005. Contrasting effects of soil development on hydrological properties and flow paths. Water Resour. Res. 41 (12).
Louvat, P., Allègre, C.J., 1997. Present denudation rates on the island of Réunion determined by river geochemistry: basalt weathering and mass budget between chemical and mechanical erosions. Geochim. Cosmochim. Acta 61 (17), 3645–3669.
Louvat, P., Allègre, C.J., 1998. Riverine erosion rates on Sao Miguel volcanic island, Azores archipelago. Chem. Geol. 148 (3–4), 177–200.
Louvat, P., Gislason, S.R., Allègre, C.J., 2008. Chemical and mechanical erosion rates in Iceland as deduced from river dissolved and solid material. Am. J. Sci. 308 (5), 679–726.
Lyons, W.B., Carey, A.E., Hicks, D.M., Nezat, C.A., 2005. Chemical weathering in high-sediment-yielding watersheds, New Zealand. J. Geophys. Res. 110 (F1), F01008.
MacKenzie, F.T., Andersson, A.J., 2013. The marine carbon system and ocean acidification during Phanerozoic time. Geochem. Perspect. 2 (1), 1–227.
Maher, K., 2010. The dependence of chemical weathering rates on fluid residence time. Earth Planet. Sci. Lett. 294 (1–2), 101–110.
Maher, K., 2011. The role of fluid residence time and topographic scales in determining chemical fluxes from landscapes. Earth Planet. Sci. Lett. 312 (1–2), 48–58.
Maher, K., Chamberlain, C.P., 2014. Hydrologic regulation of chemical weathering and the geologic carbon cycle. Science 343 (6178), 1502–1504.
Matter, J.M., Kelemen, P.B., 2009. Permanent storage of carbon dioxide in geological reservoirs by mineral carbonation. Nat. Geosci. 2 (12), 837–841.
Mehto, A., Chakrapani, G.J., 2013. Spatio-temporal variation in the hydrochemistry of Tawa River, Central India: effect of natural and anthropogenic factors. Environ. Monit. Assess. 185 (12), 9789–9802.
Mervine, E.M., Humphris, S.E., Sims, K.W.W., Kelemen, P.B., Jenkins, W.J., 2014. Carbonation rates of peridotite in the Samail Ophiolite, Sultanate of Oman, constrained through ^{14}C dating and stable isotopes. Geochim. Cosmochim. Acta 126, 371–397.
Meybeck, M., 1986. Composition chimique des ruisseaux non pollués de France. Sci. Geol., Bull., Strasbourg 39, 3–77.
Mills, B., Daines, S.J., Lenton, T.M., 2014. Changing tectonic controls on the long-term carbon cycle from Mesozoic to present. Geochem. Geophys. Geosyst. 15 (12), 4866–4884.
Misra, S., Froelich, P.N., 2012. Lithium isotope history of Cenozoic seawater: changes in silicate weathering and reverse weathering. Science 335 (6070), 818–823.
Moon, S., Chamberlain, C.P., Hilley, G.E., 2014. New estimates of silicate weathering rates and their uncertainties in global rivers. Geochim. Cosmochim. Acta 134 (0), 257–274.
Navarre-Sitchler, A., Brantley, S., 2007. Basalt weathering across scales. Earth Planet. Sci. Lett. 261 (1–2), 321–334.
Négrel, P., Deschamps, P., 1996. Natural and anthropogenic budgets of a small watershed in the massif central (France): chemical and strontium isotopic characterization of water and sediments. Aquat. Geochem. 2 (1), 1–27.
Norris, R.D., Turner, S.K., Hull, P.M., Ridgwell, A., 2013. Marine ecosystem responses to Cenozoic global change. Science 341 (6145), 492–498.
Oelkers, E.H., Gislason, S.R., 2001. The mechanism, rates and consequences of basaltic glass dissolution: I. An experimental study of the dissolution rates of basaltic glass as a function of aqueous Al, Si and oxalic acid concentration at 25 °C and pH = 3 and 11. Geochim. Cosmochim. Acta 65 (21), 3671–3681.
Oliva, P., Viers, J., Dupré, B., 2003. Chemical weathering in granitic environments. Chem. Geol. 202 (3–4), 225–256.
Pogge von Strandmann, P.A.E., et al., 2006. Riverine behaviour of uranium and lithium isotopes in an actively glaciated basaltic terrain. Earth Planet. Sci. Lett. 251 (1–2), 134–147.
Pogge von Strandmann, P.A.E., Burton, K.W., James, R.H., van Calsteren, P., Gislason, S.R., 2010. Assessing the role of climate on uranium and lithium isotope behaviour in rivers draining a basaltic terrain. Chem. Geol. 270, 227–239.
Pokrovsky, O.S., Schott, J., Kudryavtzev, D.I., Dupré, B., 2005. Basalt weathering in Central Siberia under permafrost conditions. Geochim. Cosmochim. Acta 69 (24), 5659–5680.
Prada, S., da Silva, M., Cruz, J., 2005. Groundwater behaviour in Madeira, volcanic island (Portugal). Hydrogeol. J. 13 (5–6), 800–812.
Prokushkin, A.S., et al., 2011. Sources and the flux pattern of dissolved carbon in rivers of the Yenisey basin draining the Central Siberian Plateau. Environ. Res. Lett. 6 (4), 045212.
Rad, S., Rivé, K., Vittecoq, B., Cerdan, O., Allègre, C.J., 2013. Chemical weathering and erosion rates in the Lesser Antilles: an overview in Guadeloupe, Martinique and Dominica. J. South Am. Earth Sci. 45 (0), 331–344.
Rad, S.D., Allègre, C.J., Louvat, P., 2007. Hidden erosion on volcanic islands. Earth Planet. Sci. Lett. 262 (1–2), 109–124.
Raymo, M.E., Ruddiman, W.F., Froelich, P.N., 1988. Influence of late Cenozoic mountain building on ocean geochemical cycles. Geology 16 (7), 649–653.
Rengarajan, R., Singh, S.K., Sarin, M.M., Krishnaswami, S., 2009. Strontium isotopes and major ion chemistry in the Chambal River system, India: implications to silicate erosion rates of the Ganga. Chem. Geol. 260 (1–2), 87–101.
Riebe, C.S., Kirchner, J.W., Finkel, R.C., 2004. Erosional and climatic effects on long-term chemical weathering rates in granitic landscapes spanning diverse climate regimes. Earth Planet. Sci. Lett. 224 (3–4), 547–562.
Rivé, K., Gaillardet, J., Agrinier, P., Rad, S., 2013. Carbon isotopes in the rivers from the Lesser Antilles: origin of the carbonic acid consumed by weathering reactions in the Lesser Antilles. Earth Surf. Process. Landf. 38 (9), 1020–1035.
Schaller, M.F., Wright, J.D., Kent, D.V., Olsen, P.E., 2012. Rapid emplacement of the Central Atlantic Magmatic Province as a net sink for CO_2. Earth Planet. Sci. Lett. 323–324, 27–39.
Schopka, H.H., Derry, L.A., 2012. Chemical weathering fluxes from volcanic islands and the importance of groundwater: the Hawaiian example. Earth Planet. Sci. Lett. 339–340, 67–78.
Schopka, H.H., Derry, L.A., Arcilla, C.A., 2011. Chemical weathering, river geochemistry and atmospheric carbon fluxes from volcanic and ultramafic regions on Luzon Island, the Philippines. Geochim. Cosmochim. Acta 75 (4), 978–1002.
Sharma, S.K., Subramanian, V., 2008. Hydrochemistry of the Narmada and Tapti Rivers, India. Hydrol. Process. 22 (17), 3444–3455.
Torres, M.A., West, A.J., Li, G., 2014. Sulphide oxidation and carbonate dissolution as a source of CO_2 over geological timescales. Nature 507 (7492), 346–349.

Trostle, K., Derry, L., Vigier, N., Chadwick, O., 2014. Magnesium isotope fractionation during arid pedogenesis on the island of Hawaii (USA). Proc. Earth Planet. Sci. 10, 243–248.

Van der Weijden, C.H., Pacheco, F.A.L., 2003. Hydrochemistry, weathering and weathering rates on Madeira island. J. Hydrol. 283 (1–4), 122–145.

Vitousek, P.M., et al., 1997. Soil and ecosystem development across the Hawaiian Islands. GSA Today 7 (9), 1–8.

Walker, J.C.G., Hays, P.B., Kasting, J.F., 1981. A negative feedback mechanism for the long-term stabilization of Earths surface temperature. J. Geophys. Res. 86 (C10), 9776–9782.

Wallmann, K., 2001. Controls on the Cretaceous and Cenozoic evolution of seawater composition, atmospheric CO_2 and climate. Geochim. Cosmochim. Acta 65 (18), 3005–3025.

West, A.J., 2012. Thickness of the chemical weathering zone and implications for erosional and climatic drivers of weathering and for carbon-cycle feedbacks. Geology 40 (9), 811–814.

West, A.J., Galy, A., Bickle, M., 2005. Tectonic and climatic controls on silicate weathering. Earth Planet. Sci. Lett. 235 (1–2), 211–228.

White, A.F., Blum, A.E., 1995. Effects of climate on chemical weathering in watersheds. Geochim. Cosmochim. Acta 59 (9), 1729–1747.

White, A.F., Brantley, S.L., 2003. The effect of time on the weathering of silicate minerals: why do weathering rates differ in the laboratory and field? Chem. Geol. 202 (3–4), 479–506.

Zakharova, E.A., Pokrovsky, O.S., Dupré, B., Gaillardet, J., Efimova, L.E., 2007. Chemical weathering of silicate rocks in Karelia region and Kola peninsula, NW Russia: assessing the effect of rock composition, wetlands and vegetation. Chem. Geol. 242 (1–2), 255–277.